The 8th International Supercritical CO_2 Power Cycles Symposium
February 27–29, 2024, San Antonio, Texas
Paper #107

Design of a Permanent Magnet Biased Homopolar Magnetic Bearing for sCO_2 Turbine Applications

Robert Lipham, SwRI*
Heeju Choi, PhD, Electron Energy Corporation
Marshall Bielefeld* Axon, Dongil Shin Ph.D*, General Electric Research Center (GERC)*
Erwin Thomas, Alan Palazzolo, PhD Texas A&M University
Randall Tucker* OTBOG
*Work performed while at Texas A&M

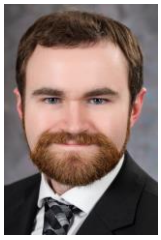

Robert Lipham is a Research Engineer at Southwest Research Institute. He specializes in rotordynamics and electromechanics.

Dr. Choi is Principal Engineer at Electron Energy Corporation. He has extensive experience in the design and control of electromechanical systems over 25 years. Especially Dr. Choi is a specialist at rare earth magnet system design using finite element analysis.

Dr. Shin is a Research Engineer at the GE Global Research Center.

Dr. Palazzolo is the James J. Cain I Professor in the Dept. of Mechanical Engineering. His research areas include magnetic bearings, conventional bearings, rotordynamics, energy storage and drilling dynamics.

Randall Tucker is the President of OTBOG Energy LLC. His specialties include custom fabrication, and engineering design for mechanical and electrical systems.

Marshall Bielefeld is a Mechanical Engineer II at Axon Enterprise.

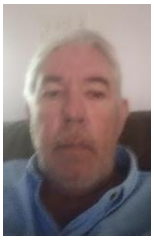

Erwin Thomas is an Electrical Engineer at Texas A&M specializing in sensor development.

ABSTRACT

The paper reports on efforts to develop a permanent magnet (PM) biased, magnetic bearing (MB) for sCO_2 turbine applications. A novel combined axial/radial, PM biased MB using unique high-temperature PMs, EEC 18-T550 produced by Electron Energy Corporation, would provide the steady bias flux for this bearing, without the large losses of electromagnet bias. Catcher (auxiliary) bearings would be included to provide shaft support in the event of a power failure or overload event of the magnetic bearings. The proposed MB technology operating at elevated temperatures +550°C and elevated pressures +2,000 psi, while providing sufficient load capacity and damping, would enable future sCO_2 turbines to operate at higher efficiencies, power densities and reliability. Studies are presented for optimizing materials for the MB and active cooling for the PMs. Desired load capacity targets are attained by increasing the PM strength through active cooling. Ultra-high-temperature position sensors are presented for feedback of shaft position in the magnetic bearing feedback loop. The presentation would provide design details, simulation results and initial test results for the combined radial/axial magnetic bearing.

INTRODUCTION

It is well recognized that bearings that can operate in sCO_2 at elevated temperatures in excess of +550°C, and elevated pressures in excess of +2,000 psi, while providing sufficient load capacity and damping, would enable future sCO_2 turbines to operate at higher efficiencies, power densities and reliability. The DOE program funded this project to develop an innovative MB and universal bearing test rig to measure load capacity, and stiffness and damping of bearings in a 700C, 4,000 psi, sCO_2 environment.

The 1st test article was planned to be a novel combined axial/radial, PM biased MB. Unique high-temperature PMs, EEC 18-T550 produced by Electron Energy Corporation, would provide the steady bias flux for this bearing, without the larger losses associated with providing electromagnet bias flux. Catcher (auxiliary) bearings were to be included to provide shaft support in the event of a power failure or overload event of the magnetic bearings.

The rig was designed to accommodate magnetic, hydrostatic and hybrid hydrodynamic /hydrostatic test bearings. The test rig design also included non-contacting, magnetic force actuators to apply static and dynamic radial and axial loads to the shaft and bearing. The relative motions of the test shaft were to be measured with specially designed high-temperature eddy current displacement sensors. These sensors would enable measurements of bearing forces to obtain stiffness and damping, along with static and dynamic journal eccentricities. An internal electric motor was planned to attain shaft speeds of 30,000 rpm or higher. sCO_2 was to be provided to the bearing test rig via high-pressure supply tanks, a sCO_2 pump and heaters. The test rig would be available at government, private or academic research labs after initial testing for aiding in the development of bearings for sCO_2 turbines and expanders.

The project was funded during the COVID-19 shelter in place era, with accompanying illness of research team members. Consequently, this precluded completion of the test rig hardware. This manuscript presents highlights of the project's design work.

RESULTS AND DISCUSSION

Magnetic Bearing Design

A combo magnetic bearing design was developed specifically for use in sCO_2 environments. This design has a homopolar, permanent-magnet (PM)-biased architecture, and it's constructed with a horizontal split to simplify assembly during testing. An overall view of the magnetic bearing and a view with the top half removed can be seen in Figure 1. A distributed axial winding, shown in purple, was developed to allow the horizontally split construction. Note that a separate stator, not shown here, is used to hold the bearing halves together. The overall dimensions are roughly 10" outer diameter by 6" axial length.

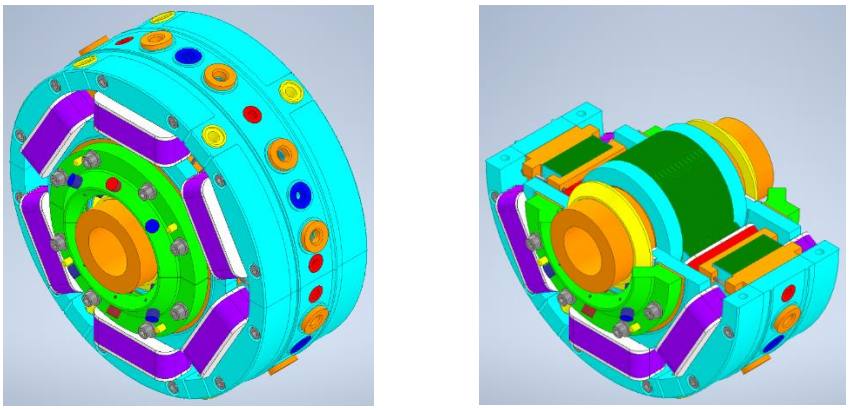

Figure 1: Views of the Magnetic Bearing. Left: Fully assembled. Right: Top half removed.

A view without the shaft and rotor laminations can be seen in Figure 2. This view better shows the catcher bearings, which are shown in white on the axial poles, and the arrangement of the radial poles.

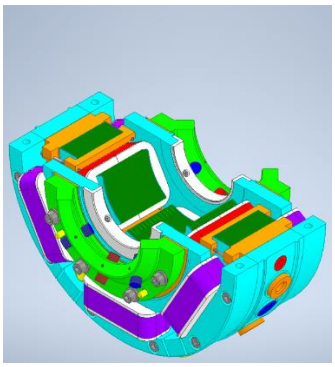

Figure 2: View of the Magnetic Bearing with Shaft Removed.

Material selection was an important aspect of this design. Of primary importance in most design decisions involved in developing sCO_2 machinery is the high temperature of the medium, and its corrosivity. However, in addition to these requirements, magnetic bearings require excellent magnetic properties. The soft magnetic materials required for magnetic bearings must have both high saturation flux density, for high force-density, and high permeability, for high force-per-ampere, in order to meet performance and footprint requirements for most applications. This leads to the common use of Fe-Co-V alloys, commonly known by the tradename Hiperco®, since

they provide some of the highest saturation flux densities and permeabilities of any commercially available alloy. The curie temperatures of these alloys also typically exceed 900 °C, which coincidentally makes these alloys useful in high-temperature applications like sCO_2. For these reasons, Hiperco® alloys were selected for this design. The hard magnetic materials required for PM-biased magnetic bearings must have high residual flux density for high force-density. Combined with the high temperature requirements of sCO_2, this led to the selection of SmCo alloys for this design.

One of the primary challenges involved in this design effort stemmed from the high operating temperatures required for sCO_2, and the conflicting need to keep the bearing cool for better magnetic performance. The selection of Hiperco® for the soft materials in this bearing mitigated some of these issues. However, while some blends of SmCo used in permanent magnets can handle temperatures around 550 °C, the residual flux density of this material has a strong negative correlation with temperature. This can lead to performance degradation of the magnetic bearing if the PMs are not kept at relatively cooler temperatures. This issue was tackled with the inclusion of active cooling to keep the temperature of the PMs within their preferred operating region of roughly 100 °C–200 °C. Low-temperature sCO_2 was selected as the cooling medium in order to avoid contamination of the process medium. As an added benefit of using lower-temperature sCO_2 as a cooling medium, the more corrosive, higher-temperature sCO_2 can be kept out of the internals of the magnetic bearing.

Magnetic Bearing Controller Design

Controller design is as important to magnetic bearing performance as the design of the actuator itself. Equally important to the design of the controller is the shaft position feedback method. While there are examples of sensorless control schemes, most employ proximity sensors to directly measure shaft position. In low-temperature applications, the shaft position for a combo bearing can be measured by as few as two radial probes and one axial probe. However, in high-temperature applications, thermal growth of both the probe mounting fixture and shaft can add offsets to any calibration done at room temperature. Therefore, for this application, it was decided to use opposing probes to cancel out thermal growth effects. In addition, in order to aid characterization of the bearing in a testing environment, it was decided to use two radial probe planes and several opposing axial probes. This led to an initial probe layout similar to that of Figure 3.

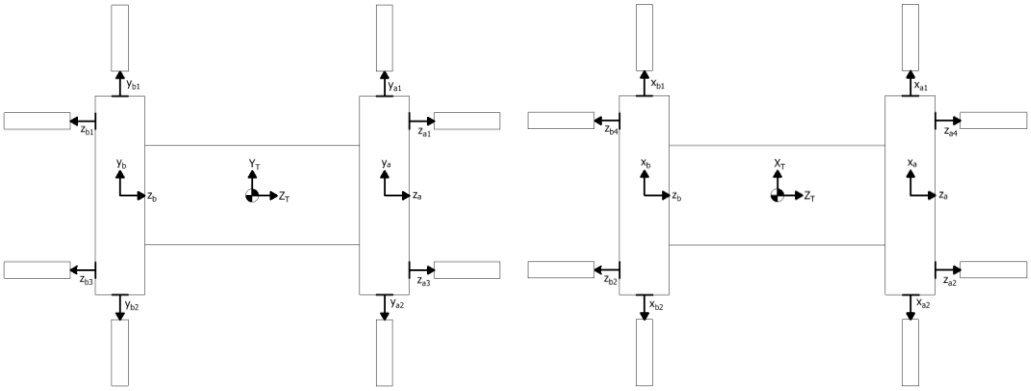

Figure 3: Uncoupled Probe Configuration. Left: Y-Z plane. Right: X-Z plane.

This is a fairly conventional probe layout, and the math for determining shaft position is fairly straightforward. These equations are summarized in eqs. 1–3, and they effectively act as an average of the probe inputs for each axis.

$$X_T = \frac{1}{4}\big(G_{xa1}(V_{xa10} - V_{xa1}) - G_{xa2}(V_{xa20} - V_{xa2}) + G_{xb1}(V_{xb10} - V_{xb1}) - G_{xb2}(V_{xb20} - V_{xb2})\big) \quad (1)$$

$$Y_T = \frac{1}{4}\Big(G_{ya1}\big(V_{ya10} - V_{ya1}\big) - G_{ya2}\big(V_{ya20} - V_{ya2}\big) + G_{yb1}\big(V_{yb10} - V_{yb1}\big) - G_{yb2}\big(V_{yb20} - V_{yb2}\big)\Big) \quad (2)$$

$$Z_T = \frac{1}{8}\sum_{n=1}^{4}\big(G_{zan}(V_{zan0} - V_{zan}) - G_{zbn}(V_{zbn0} - V_{zbn})\big) \quad (3)$$

Note that “G” denotes a probe gain, and the subscript “0” denotes an offset voltage. One feature of note is that the thermal growth cancelling behavior is immediately demonstrated in these equations. If, for example, each of the probes in the z-axis see a perturbation of δ_{zt} due to thermal growth while the shaft is centered, and we assume unity gains and zero offset voltages, then the resulting z-axis position can be described by 4.

$$Z_T = \frac{1}{8}\sum_{n=1}^{4}\big((-\delta_{ztn}) - (-\delta_{ztn})\big) = 0 \quad (4)$$

One downside of this probe arrangement is that is adds axial length to the magnetic bearing due to the second set of axial probes. This was seen as particular issue for the test rig this bearing was developed for since it increased overall shaft length and component spacing requirements inside the containing pressure vessel. An alternative probe configuration was developed to help reduce the axial length of the assembly. This arrangement, shown in Figure 4 , utilizes a set of coupled probes oriented at 45° to the shaft axis.

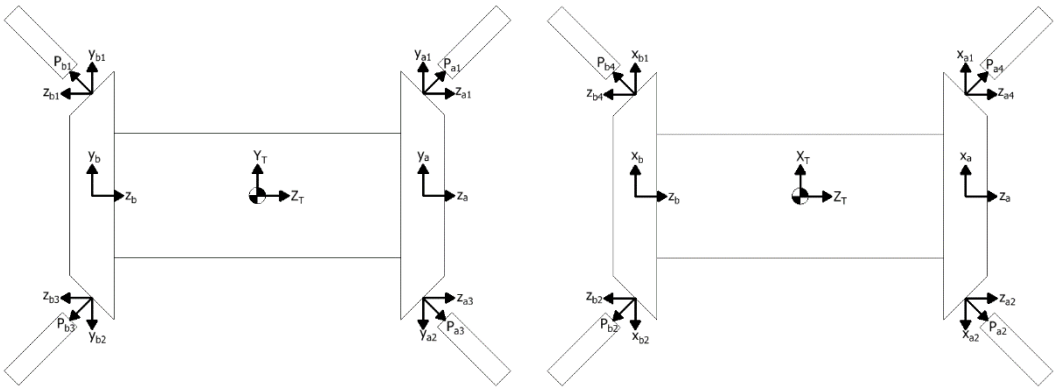

Figure 4: Coupled Probe Configuration. Left: Y-Z plane. Right: X-Z plane.

An added benefit of this arrangement is a lower probe count, 8 total, than would be possible with a fully uncoupled arrangement. Even if the arrangement in Figure 3 were limited to two opposing axial probes, the count would still be 10 total probes. One downside of this probe arrangement

is the potential change in probe gain due to the conical target surface. While this would require additional calibration steps for a commercial probe, the custom probes being developed for this rig were already being calibrated in-situ, so this was not seen as a major disadvantage. While the math for determining shaft position involves a few more vector projections than the previous probe arrangement, the resulting equations have the same form as the uncoupled probe arrangement. This can be seen in eqs. 5–7.

$$X_T = \frac{\sqrt{2}}{2} \cdot \frac{1}{4}\big(G_{a4}(V_{a40} - V_{a4}) - G_{a2}(V_{a20} - V_{a2}) + G_{b4}(V_{b40} - V_{b4}) - G_{b2}(V_{b20} - V_{b2})\big) \tag{5}$$

$$Y_T = \frac{\sqrt{2}}{2} \cdot \frac{1}{4}\big(G_{a1}(V_{a10} - V_{a1}) - G_{a3}(V_{a30} - V_{a3}) + G_{b1}(V_{b10} - V_{b1}) - G_{b3}(V_{b30} - V_{b3})\big) \tag{6}$$

$$Z_T = \frac{\sqrt{2}}{2} \cdot \frac{1}{8}\sum_{n=1}^{4}\big(G_{an}(V_{an0} - V_{an}) - G_{bn}(V_{bn0} - V_{bn})\big) \tag{7}$$

With position feedback available, there are several valid approaches for magnetic bearing control that depend on the application in question. For the testing application that this bearing was developed for, it was decided to use three decoupled, single-input-single-output (SISO) controllers. This was seen as a valid approach since this bearing would be acting in isolation to the rest of the test rig. An example of one of these control loops is shown in Figure 5.

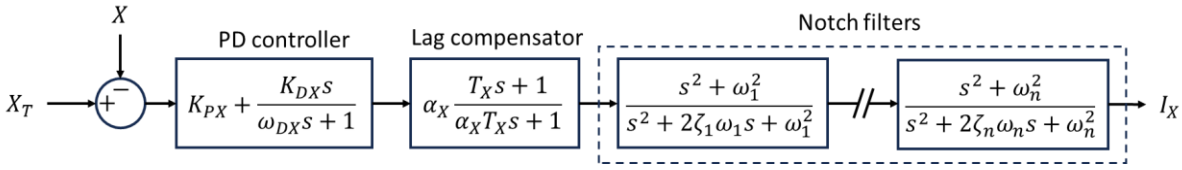

Figure 5: Example SISO Controller

A standard filtered PD controller was selected for primary error correction to allow for tuning of both stiffness and damping, and lag compensation was included for reducing steady-state error. Due to the redundant radial control axes, the control current outputs of the x-axis and y-axis SISO controllers must be converted into A, B, and C-axis control currents before being sent to the bearing amplifiers. The axis definitions can be found in Figure 6, and the transformation matrix for this operation is described in Y8.

$$\begin{bmatrix} I_A \\ I_B \\ I_C \end{bmatrix} = \frac{1}{2}\begin{bmatrix} -\sqrt{3} & 1 \\ 0 & 2 \\ \sqrt{3} & 1 \end{bmatrix}\begin{bmatrix} I_X \\ I_Y \end{bmatrix} \tag{8}$$

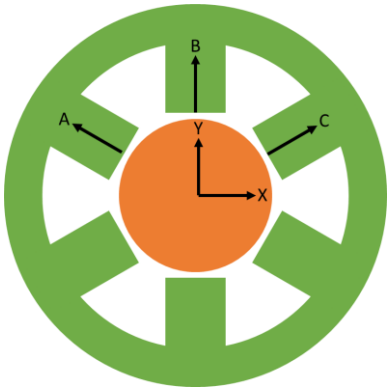

Figure 6: Radial Axis Definitions

Magnetic Bearing Performance Simulations

Magnetostatic simulations were performed with this design to estimate axial and radial load capacity. Material assignments were made as previously described. The SmCo magnets were assumed to have average temperatures of 100°C due to the active cooling system. The Hiperco® laminations and back-iron were assumed be in this temperature range due to both the effects of the active cooling medium inside the bearing and the insulating material included on the separating can surrounding the bearing.

Three types of parametric studies were performed during these simulations. The first type of study estimated bearing forces for a given input current while the shaft was at the center of the bearing. This was used to characterize current stiffness and maximum output force at shaft center. The second type of study estimated bearing forces for a given input current while the shaft was displaced -20 mils from the center of the bearing. This was used to characterize the worst case (greatest clearance) liftoff force of the bearing when the shaft was resting on the catcher bearings. The third type of study estimated bearing forces over a range of shaft positions while the input current was set to zero. This was used to characterize the negative position stiffness of the bearing. All three types of parametric study were independently performed on both the y-axis (radial) and z-axis (axial) of the bearing. That is to say, while one axis was studied, the control current and shaft position of the other axis were held at zero. The results of these simulation studies can be seen in Figures 7–10. A summary of these simulation studies and the resulting estimated bearing parameters can be found in Table 1.

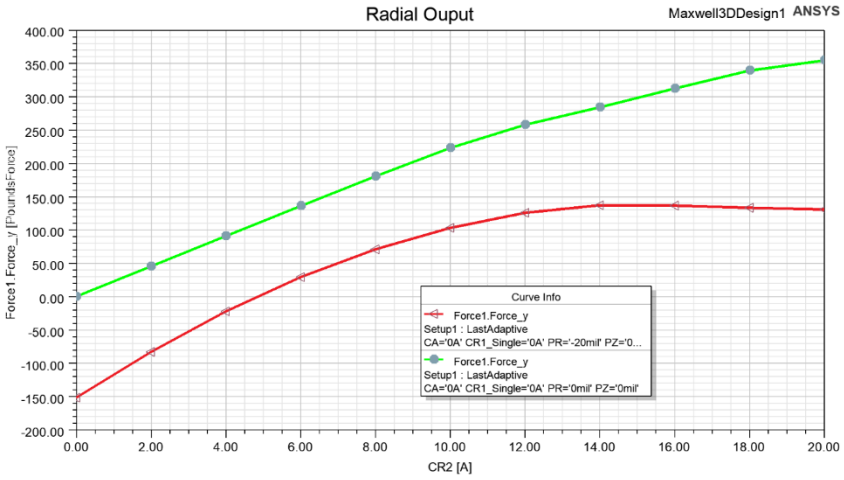

Figure 7: Predicted Radial Force Output. Green Line: Force from center. Red Line: Force from -20 mils radial offset.

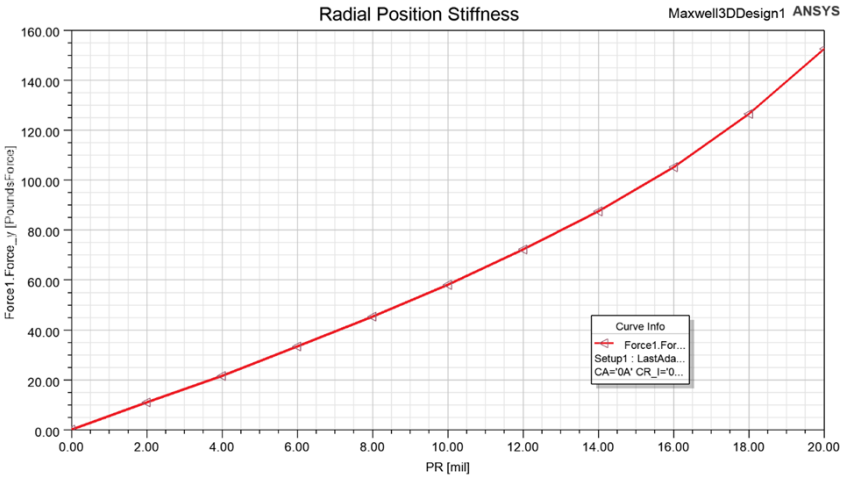

Figure 8: Predicted Radial Position Stiffness with Zero Input Current

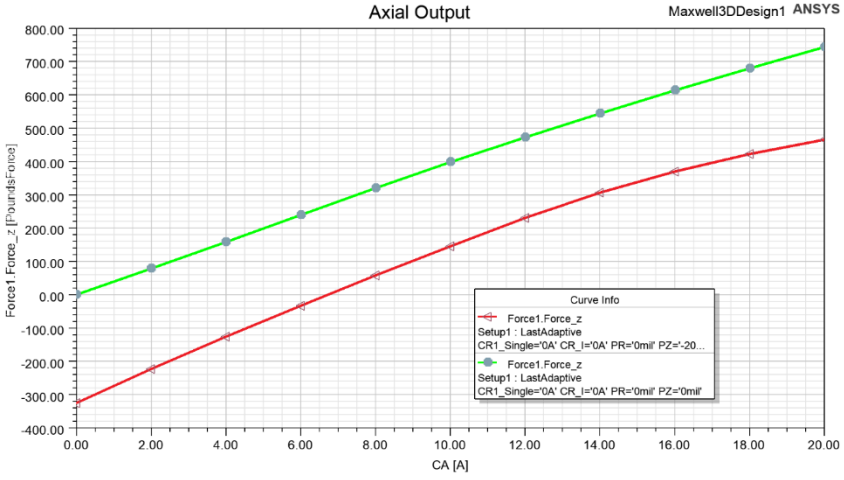

Figure 9: Predicted Axial Force Output. Green Line: Force from center. Red Line: Force from -20 mils axial offset.

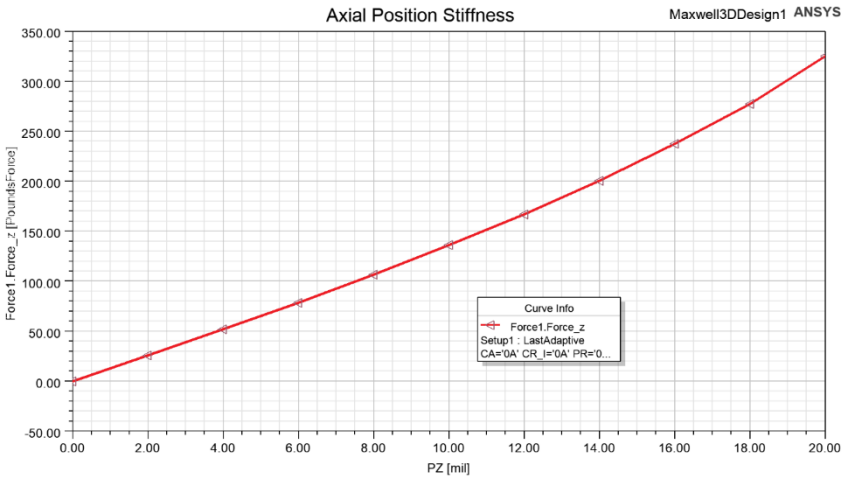

Figure 10: Predicted Axial Position Stiffness with Zero Input Current

Table 1: Summary of Simulated Magnetic Bearing Performance

Output	Current Stiffness at 10 A	Position Stiffness at 6 mils	Liftoff force from -20 mils at 10 A	Max Centered Force at 20 A
Radial	22.5 lbf/A	5,830 lbf/in	100 lbf	350 lbf
Axial	40 lbf/A	13,300 lbf/in	150 lbf	740 lbf

Active Cooling System Design

The permanent magnets in the Combo magnetic bearing lose strength as temperature increases. Therefore, the design incorporates an active cooling system to lower the PM temperatures. The CHT model provides temperature fields within the solid and fluid components of the model. Figure 11 shows that the PM magnetic strength weakens as the magnetic temperature increase. The figure demonstrates that the magnetic strength can be considerably increased by cooling the magnet from 550°C or higher to 200°C or lower.

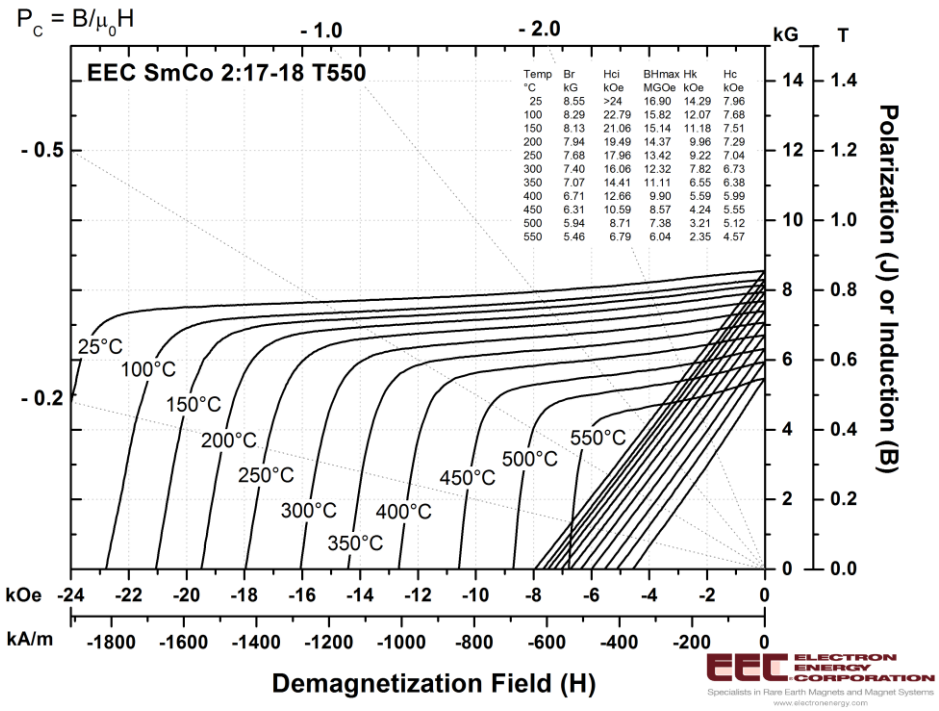

Figure 11*:* EEC Magnets B/H curves

A study was then conducted to determine the ideal working fluid to cool the PMs. This was done by directly comparing the results of a series of tests comprised of air, nitrogen and sCO_2 as the cooling medium. It is important to note the boundary conditions and reference properties used in these analyses:

- Exterior Surface set to 700 °C
- Zero Leakage (mass flow of inlets == mass flow of outlets)
- Fixed Exit Pressure
- Fixed Inlet Temperature
- Fixed Inlet Flow Rate

Reference Properties

The sCO_2 and N_2 simulations shown below utilize reference property tables to accurately model these gasses. These real gas property tables are created from a .FLD file and written to an RGP file which is a NIST type file. RGP files can then be read by ANSYS CFX to model the fluid. RGP tables utilize equations of state to model dynamic properties such as density that vary greatly with changes in temperature and pressure. This is especially important for dynamic material like sCO_2. Figure 12 shows a general temperature vs pressure graph of CO_2.

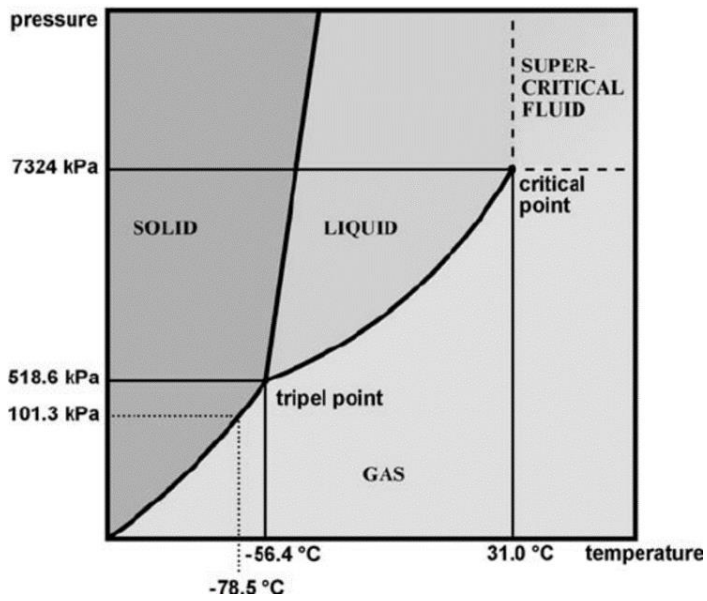

Figure 12: Niessen, Heiko & Woelk, Klaus. (2005). Investigations in Supercritical Fluids. 10.1007/b135837.

Air Cooling

The first simulation was conducted using air cooling to keep the magnets within their operating temperature and acts as a base value for the other analyses. In the current model, ambient air would be pumped in axially from both sides of the bearing and then exit radially outward. The key results of the air-cooling simulation are tabulated below. Issues found with using air were the high volumetric flow rate required and the large pressure differential between the interior and exterior of the bearing. Additionally, at the mass flow rate used for this initial test, the fluid failed to bring the PMs to the desired sub-200°C average temperature. The use of other coolants was then explored.

Table 2: Combo Bearing Active Air-Cooling Results

Mass Flow Rate Total	0.025 lbm/s
Volumetric Flow Rate Inlet	203 cfm
Average Inlet Air Temperature	25 °C
Average Outlet Air Temperature	312 °C
Average Pressure	14.7 psi
Average Lamination Temperature	654 °C
Maximum Magnet Temperature	382 °C
Average Magnet Temperature	282 °C
Magnet Br	0.75 T
Magnet Hc	-6.8 kOe

sCO_2 vs N_2 Cooling @75°C

Shown below in Table 3 and Figure 13, are the results of an sCO_2 cooled and an N_2 cooled bearing using the same boundary conditions, for direct comparison. One major difference between the 2 simulations is the change in volumetric flow rate. Due to the inlet density difference between N_2 and sCO_2, the volumetric flow rate of N_2 is roughly 3x that of sCO_2.

Additionally, less overall cooling is obtained when using N_2 resulting in a difference in average magnet temperature of 44°C. The pressure used was later determined to be higher than the typical approximately 1500 psi projected to be present at the exhaust end of sCO_2 turbines.

Table 3: Combo Bearing Active sCO_2 and N_2 Cooling Results for 75°C Inlet Coolant

	sCO_2 @75°C	N_2 @75°C
Mass Flow Rate Total	0.025 lbm/s	0.025 lbm/s
Volumetric Flow Rate Inlet	0.035 cfm	0.103 cfm
Average Inlet sCO_2 Temperature	75 °C	75°C
Average Outlet sCO_2 Temperature	214 °C	272 °C
Average Pressure	4000 psi	4000 psi
Average Lamination Temperature	626 °C	632°C
Maximum Magnet Temperature	160 °C	205 °C
Average Magnet Temperature	156 °C	200 °C
Magnet Br	0.81 T	0.79 T
Magnet Hc	-7.5 kOe	-7.3 kOe

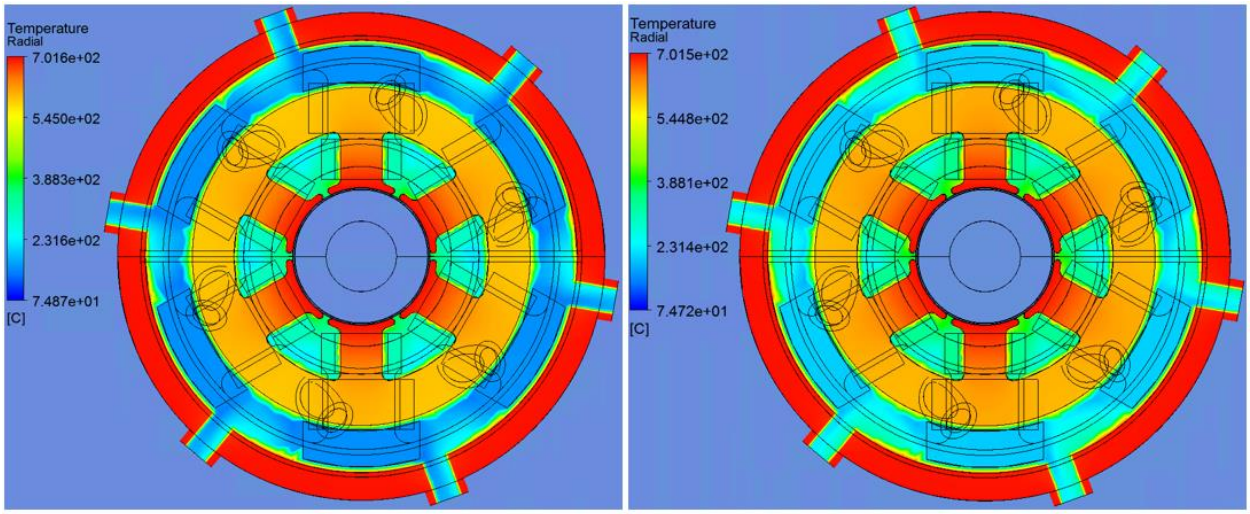

SCO2 @75°C N2 @75°C

Figure 13*:* sCO_2 vs N_2 thermal distribution at 75°C inlet

sCO_2 vs N_2 Cooling @250°C

Shown below in Table 4 and Figure 14 are the results of an sCO_2 cooled and an N_2 cooled bearing using the same boundary conditions for direct comparison. However, using a higher inlet temperature has caused N_2 and sCO_2 to output more similar values in terms of volumetric flow rate and overall cooling. In terms of required volumetric flow rate, N_2 is still 2x that of sCO_2; however, the difference in average magnet temperature reduced to 15°C.

Table 4: Combo Bearing Active sCO_2 and N_2 Cooling Results for 250°C Inlet Coolant

	sCO_2 @ 250°C	N_2 @ 250°C
Mass Flow Rate Total	0.025 lbm/s	0.025 lbm/s
Volumetric Flow Rate Inlet	0.080 cfm	0.155 cfm
Average Inlet sCO_2 Temperature	250 °C	250 °C
Average Outlet sCO_2 Temperature	389 °C	405 °C
Average Pressure	4000 psi	4000 psi
Average Lamination Temperature	647 °C	650°C
Maximum Magnet Temperature	345 °C	360°C
Average Magnet Temperature	341 °C	356 °C
Magnet Br	0.72 T	0.7 T
Magnet Hc	-6.5 kOe	-6.3 kOe

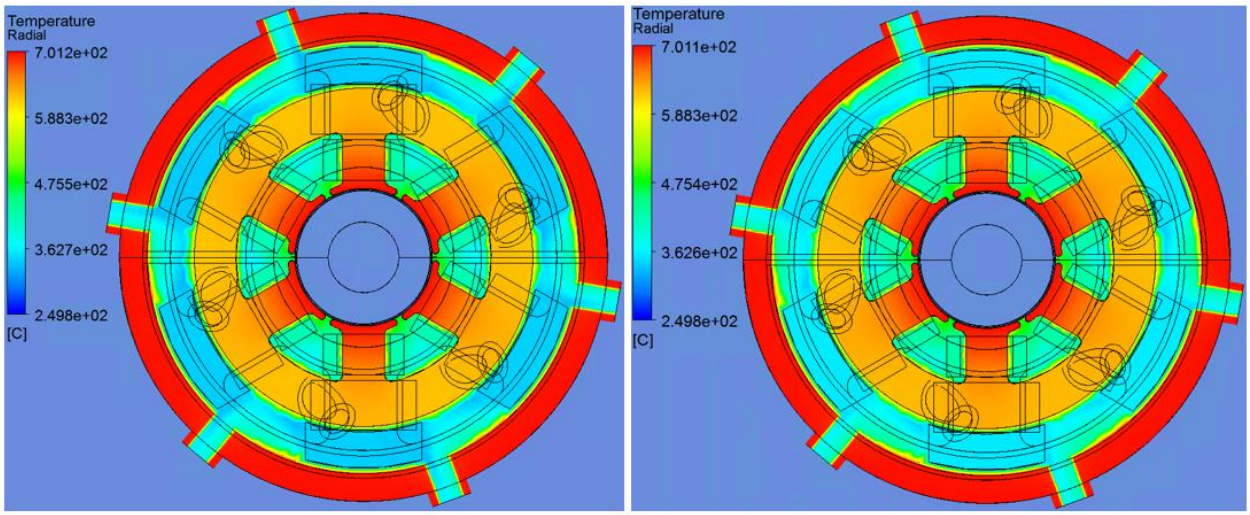

SCO2 @250°C N2 @250°C

Figure 14*:* sCO_2 vs N_2 thermal distribution at 250°C inlet

3000 psi vs 4000 psi sCO_2 @75°C

From the results of the previous tests, it was determined that using sCO_2 as the working fluid would be ideal. This is due greatly to the relatively high energy density of sCO_2. Additionally, utilizing the same fluid to cool the PMs as exists outside the bearing simplifies the overarching mechanism. Further tests were then performed to determine the effects of fluid pressure on cooling effectivity. Shown below are the results of cooling when using 3000psi and 4000 psi sCO_2. Current building constraints may limit the maximum achievable internal pressure to 3000 psi; therefore, it is important to determine the resulting cooling changes. For this comparison, the volumetric flow rate was kept constant at 1 liter per minute.

Table 5: Combo Bearing Active sCO_2 Cooling with 75C, 3,000 and 4,000 psi Inlet Coolant

	sCO_2 @3000psi	sCO_2 @4000psi
Mass Flow Rate Total	0.018 lbm/s	0.025 lbm/s
Volumetric Flow Rate Inlet	0.035 cfm or 1 L/min	0.035 cfm or 1 L/min
Average Inlet sCO_2 Temperature	75 °C	75 °C
Average Outlet sCO_2 Temperature	221 °C	214 °C
Average Pressure	3000 psi	4000 psi
Average Lamination Temperature	656 °C	626 °C
Maximum Magnet Temperature	160 °C	160 °C
Average Magnet Temperature	156 °C	156 °C
Magnet Br	0.81 T	0.81 T
Magnet Hc	-7.5 kOe	-7.5 kOe

Shown below in Figure 15 are the raw results from ANSYS CFX simulation for the 3000psi sCO_2 test tabulated above.

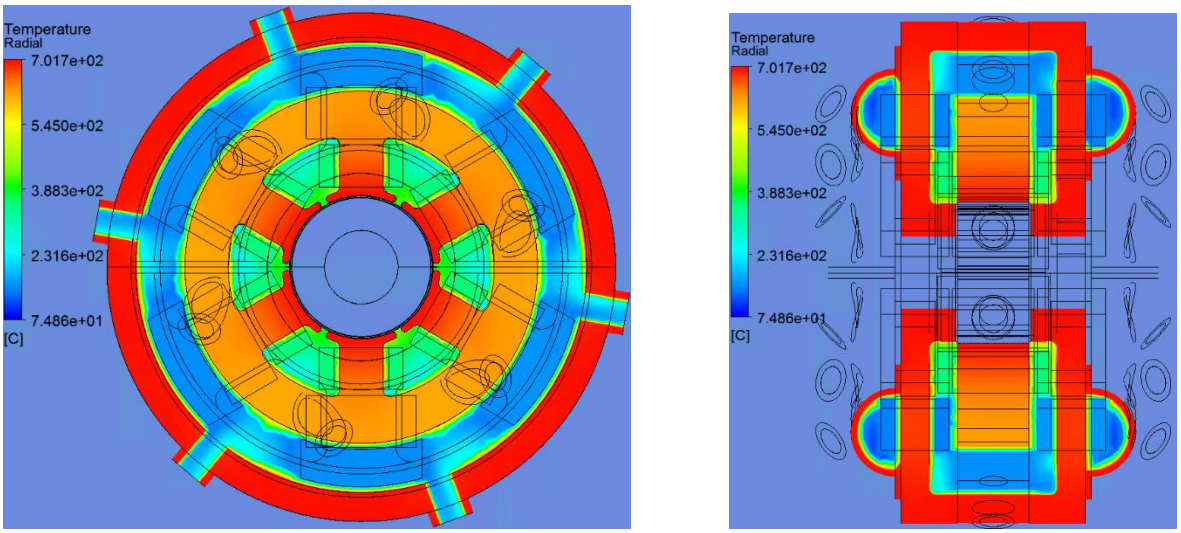

Figure 15*:* sCO_2 Coolant Inlet @3000psi & 75°C. Radial and Axial Temperature Distributions

1 liter/min vs 4 liter/min sCO_2 @3000 psi & 75°C Coolant Flow

Table 6 shows the results for a sCO_2 cooling simulation utilizing 4 liters per minute of flow. The purpose of this run was to determine if increasing the flow rate resulted in a significant increase in overall performance. As such, it is compared side by side with the previously mentioned sCO_2 case at 3000psi.

Table 6: Combo Bearing Active sCO_2 Cooling with 75C, 3,000 psi, 1 liter/min and 4 liter/min Inlet Coolant

	sCO_2 @1 L/min	sCO_2 @4 L/min
Mass Flow Rate Total	0.018 lbm/s	.073
Volumetric Flow Rate Inlet	0.035 cfm or 1 L/min	0.141 cfm or 4 L/min
Average Inlet sCO_2 Temperature	75°C	75°C
Average Outlet sCO_2 Temperature	221°C	181°C
Average Pressure	3000 psi	3000 psi
Average Lamination Temperature	656 °C	596 °C
Maximum Magnet Temperature	160 °C	136 °C
Average Magnet Temperature	156 °C	132°C
Magnet Br	0.81 T	0.82 T
Magnet Hc	-7.5 kOe	-7.6 kOe

Cooling Results

The result of the thermal study was that sCO_2 is the ideal working fluid of those tested for cooling of the PMs and interior of the combo bearing. The major advantage of using sCO_2 is its relatively high energy density; thereby, resulting in high amounts of cooling at low flow rates. Additionally, at working temperatures, the fluid can be pressurized to match the exterior pressure. This significantly reduces stress on the exterior shell of the combo bearing. Finally, using the same fluid to cool the bearing as is being worked in the turbine reduces the complexity of the fixture and minimizes the issue of leakage out of the bearing. Introducing N_2 into an sCO_2 loop is undesirable.

Catcher Bearing Design

The Catcher Bearing (CB) is integral to the magnetic bearing system, providing essential protection to the rotor-bearing systems against damage resulting from a rotor drop. In the event of a power outage causing the failure of the rotor with a magnetic bearing system, a rotor drop occurs, impacting the inner surface of the catcher bearing parts. This drop event generates a significant contact force between the shaft and catcher bearing, presenting the risk of damage to both the catcher bearing and rotor systems. Rotor drop simulation is performed to assess the safe operation of the Universal Bearing Test Rig rotor in the event of power failure. The conceptual model of the shaft is shown on the left in Figure 16, and the combo bearing design with two catcher bearings is shown on the right in Figure 16.

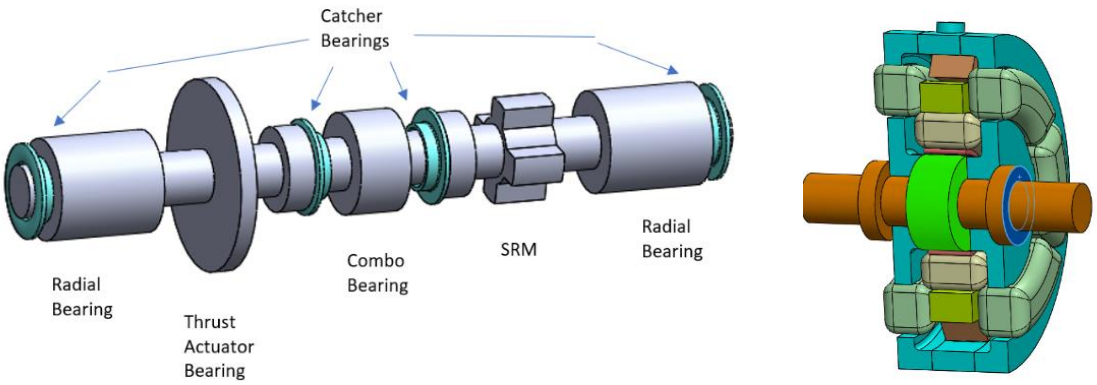

Figure 16: Left: Concept Design of Universal Bearing Test Rig Shaft. Right: Combo Bearing Design with two catcher bearings.

To mitigate the potential damage in the absence of magnetic bearing force, four catcher bearings are installed in the shaft, and their locations are shown in Figure 16. The clearance between the shaft and catcher bearing is set at 0.007 inches. Tangential force arises when the shaft comes into contact with the bearing sleeve, presenting the risk of a destructive backward whirl of the journal. To determine the tangential force during contact, a friction coefficient of 0.05 is used between the shaft and the bearing sleeve. The rotating speed of the rotor when the rotor

drop starts is set at 30,000 rpm. The shaft model is formulated using Euler beam theory, incorporating four degrees of freedom at each node. The initial conditions for the rotor drop event are set at the bearing clearance center, and the simulation is carried out for a duration of 0.5 seconds.

In Figure 17, the trajectories of the shaft during the rotor drop event are depicted at the four catcher bearing locations. In each scenario, the rotor descends initially when dropped from the clearance center. Following the occurrence of contact between the rotor and the bearing sleeve, the rotor undergoes an upward movement in conjunction with the bearing sleeve surface, eventually converging to equilibrium points. The results shows that at all catcher bearing locations, the shaft maintains a stable vibration level throughout the rotor drop event. These results confirm that the current conceptual design of the shaft-catcher bearing is effective in preventing damages caused by the rotor drop during a power outage of the magnetic bearing. In addition, no backward whirl is identified from the simulation at all four catcher bearing locations.

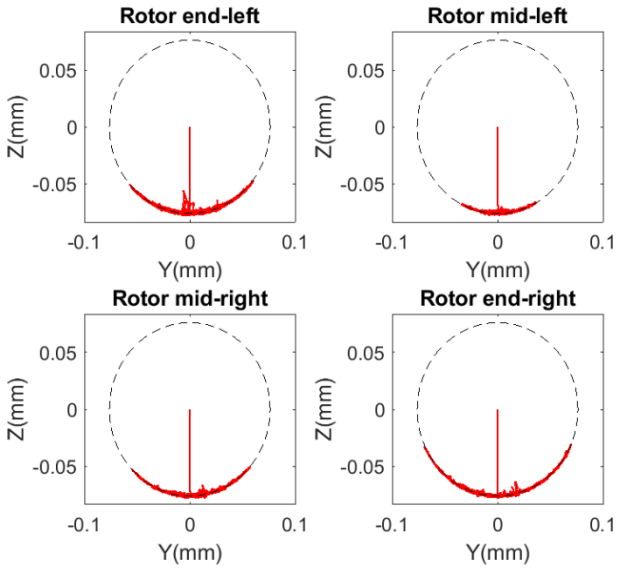

Figure 17: Rotor Orbits in Drop Simulation

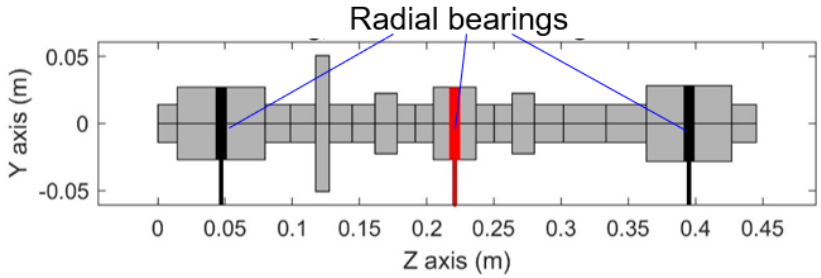

Figure 18: Finite Element Model of Shaft with three radial bearings

Rotordynamics

As shown in Figure 18, the shaft is supported in the y-axis direction by three radial bearings, while four catcher bearings are positioned at both axial ends and mid-planes of the shaft. A thrust bearing with a diameter of 4.5 inches is incorporated between the left radial and mid-combo bearings in the shaft. The overall dimensions of the shaft measure approximately 17.5 inches in length and 1.25 inches in diameter. This was for a sub-scale test rig and not for an industrial unit. The finite element model based on the Euler beam theory is depicted in Figure 18. For the sake of analysis simplicity, the bearing stiffnesses for all three bearings are assumed to be the same, with a range varying from 2,000 lb/in to 30,000 lb/in during the simulation.

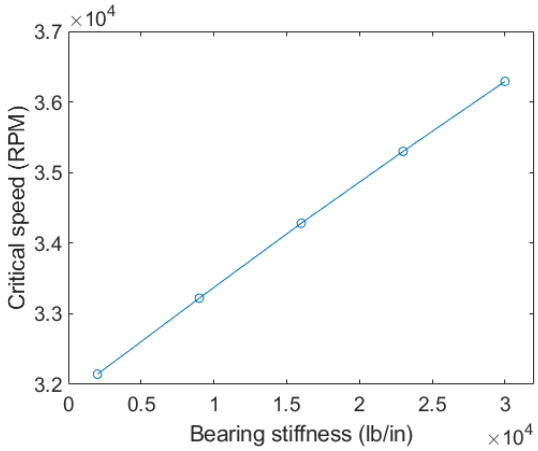

Figure 19: Critical Speed vs. Bearing Stiffness

The critical speeds of the developed rotor-bearing system with different bearing stiffness values are illustrated in Figure 19. At the lowest bearing stiffness of 2000 lb/in, the calculated critical speed of the rotor is 32,612 rpm. As the bearing stiffness increases, the critical speeds increase accordingly, reaching a maximum of 36,300 rpm at a bearing stiffness of 30,000 lb/in.

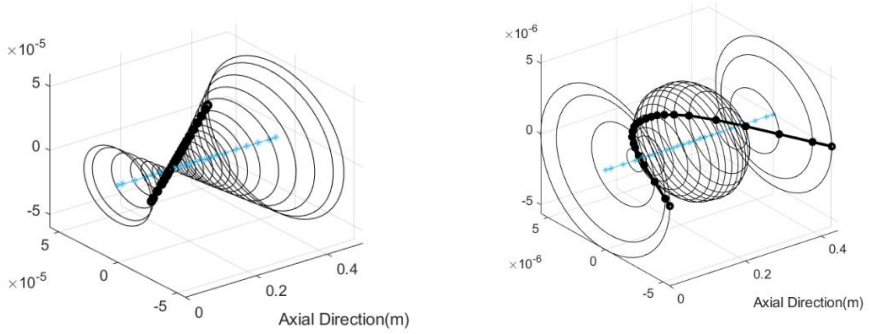

Figure 20: Rotor Mode Shapes with bearing stiffness of 2,000 lb/in. Left: Rigid body mode (7,180 RPM). Right: Flexible bending mode (32,612 RPM).

The mode shapes corresponding to the bearing stiffness of 2,000 lb/in are depicted in Figure 20. At 7,180 rpm, a rigid body mode with a conical shape is illustrated in Figure 20. At 32,612 rpm, the flexible bending mode shape emerges, characterized by significant deflections at both ends and the midpoint of the shaft, as shown in Figure 20. The 2nd rigid body mode was not excited by the imbalance distribution used in the simulation presented in Fig. 21.

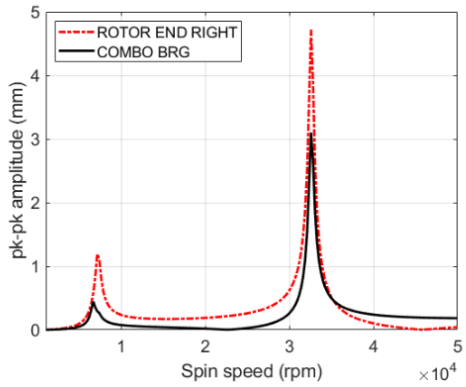

Figure 21: Unbalance Responses of developed Rotor-bearing system

The unbalance responses of the rotor-bearing system are illustrated in Figure 21, with bearing stiffnesses set at 9,000 lb/in and bearing damping at 103 lbf/in for the calculations. In Figure 21, the unbalance responses at the shaft's right end and combo bearing nodes are displayed. A minor vibration peak around 7,000 rpm is observed, attributed to rigid body motion. Moreover, significant peak-to-peak vibrations are seen to occur above 30,000 rpm at both the shaft-end and shaft-mid locations.

Magnetic Bearing Test Rigs

Figure 22 shows an illustration of the PM Radial MB and test fixture for high temperature, applied static load levitation testing. The test fixture would be placed in the Olympic FL10E radiant kiln furnace shown in Figure 23, at a temperature of 1300 F (700 C). The interior dimensions are 24” x 24” x 30” with the fires to cone being 10/2350 °F. The kiln would be used to cure and test the ultra-high-temperature (UHT) magnetic bearing, backup bearing and sensor components, and low-speed test the Phase II test rig. Hole drilling is being planned through the top and bottom of the kiln to accommodate wires and pipes for the UHT PM MB . This is acceptable because the heating elements are along the sides.

Preliminary tests have been conducted on wire samples at 800 °C. In this test, the insulation performed well. The resistance changed as expected with a factor of 3 increase from room temperature to 800 °C. A similar test was conducted on the 1008 steel laminations to determine the survivability of the insulation coating them. From this test it was determined that C5 coating was a suitable insulation for the situation.

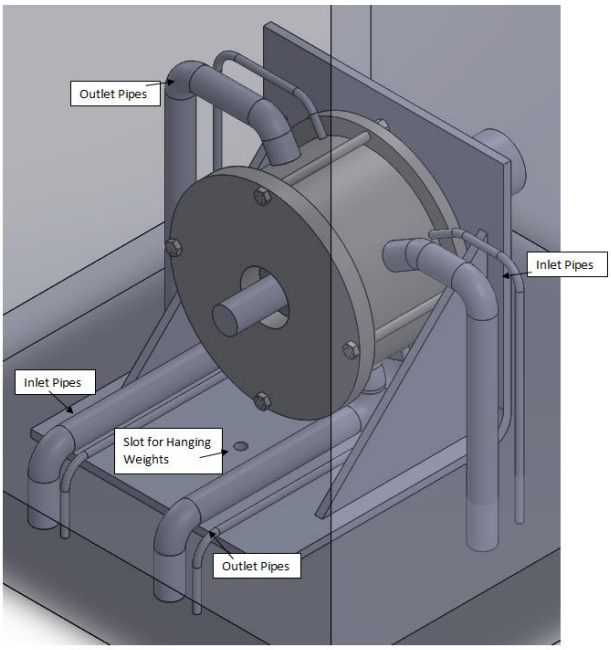

Figure 22: PMRMB mounted in a test fixture for high-temperature, applied load, levitation testing

Figure 23**:** PMRMB test chamber Olympic FL10E radiant kiln furnace

We developed an initial design for the originally proposed Phase II demonstration test rig for the UHT-PM-MB actuators, sensors and auxiliary bearings. Rotordynamics for critical speed, stability and imbalance response and transient rotor drop onto the auxiliary bearings was analyzed in detail and are shown in the previous section.

Low-Cost, Ultra-High-Temperature, Shaft Position Sensor Development

The high-cost and 550°C limit of commercially available shaft position sensors, for magnetic levitation, necessitates development of reasonably priced ultra-high-temperature alternatives. Optimally the sCO_2 turbines would have 20 shaft position sensors which, if purchased commercially, may cost $200,000 and be limited to 550°C max temperature. The need for a large number of sensors is the presence of shaft out of roundness (runout) which causes false

motion signals to enter into the magnetic bearing control feedback.

Figure 24 depicts an 8 radial sensor array for shaft positioning sensing and runout reduction. Thus, a dedicated effort was made in Phase I to develop a low-cost, 700°C rotating shaft position sensor system. Modeling, simulation, test, design and fabrication steps were completed to achieve this goal. The photos in Figure 25 show a test setup with a target shaft in a small kiln, and a micrometer mounted test sensor that can move radially towards or away from the shaft in the 700°C environment. The sensor drive electronics were initially developed on a bread board and transferred to a custom built printed circuit board. Although the high-temperature calibration plot shown in Figure 26 shows excellent range and linearity, a significant DC drift problem is occurring and would be resolved in the Phase II work.

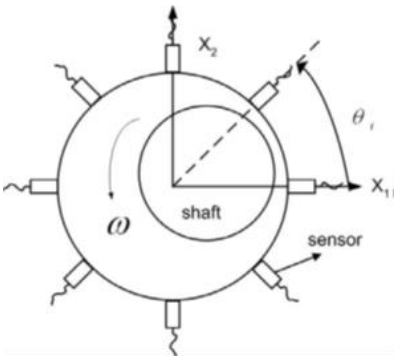

Figure 24: Eight radial sensor array for shaft positioning sensing and runout reduction.

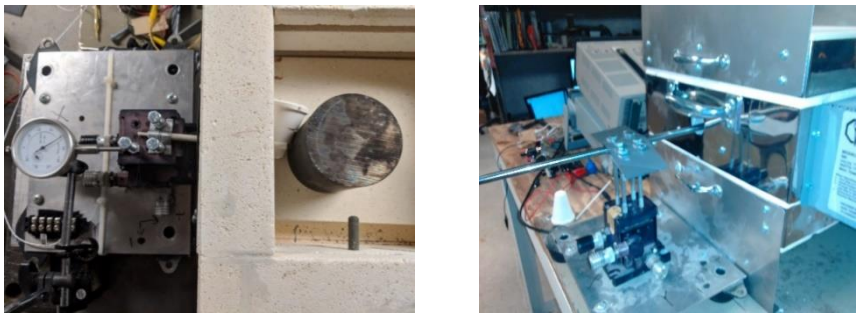

Figure 25: High-temperature sensor testing rig. Left: Translation stage for advancing sensor into target shaft. : Right Sensor holder advancing through kiln wall into hot zone.

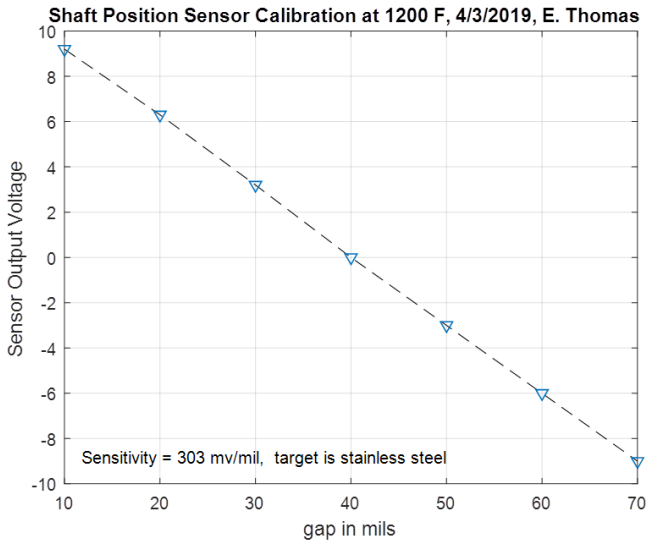

Figure 26: High-temperature calibration curve

Universal sCO_2 Bearing Test Rig

The purpose of the Universal sCO_2 Bearing Test Rig (USBTR) is to provide a test platform for measuring the load capacity, stiffness and damping of gas or magnetic bearings, for use in sCO_2 Turbines and Turboexpanders. The planned operating environment for the test bearings is 1200 F–1300 F, 3,000–4,000 psi, sCO_2. The first test bearing would be a combo (combined radial and axial) magnetic bearing with permanent magnet bias and active cooling. Radial magnetic bearings positioned at the top and bottom of the test rig, and an axial magnetic bearing, would apply static and dynamic loads on the test bearings. These loads would enable the measurement of the test bearing's load capacity and stiffness and damping. The load measurement system would utilize mounting of the test bearing on compliant supports with known stiffness, and measurement of the test bearing's displacements and accelerations.

The USBTR would have an integral, internal switched reluctance motor to spin the rotor up to 30,000 rpm. This configuration would permit testing of the following bearing types for load capacity and stiffness and damping:

- Radial hydrostatic, hydrodynamic or hybrid gas bearings including plain journal, pocketed, or foil bearings
- Axial hydrostatic, hydrodynamic, or hybrid gas bearings
- Radial, axial, or combination magnetic bearings

The USBTR would also have an integral, built in electric lift system to facilitate maintenance and inspection of the rig and test bearing replacement.

The project was simultaneously developing an sCO_2 autoclave and test facility along with the USBTR. The autoclave would be used to determine the corrosion and oxidation characteristics of materials for planned use in the rig. The autoclave would be operated in the 3000–4000psi, 1200F–1300 F range with sCO_2. The facility would include a flow system, sCO_2 pump and heaters. The test rig would be located in a shipping container for safety purposes, and the corresponding control room would be located in a nearby, air-conditioned safety container.

The main safety features of this design would be that the system is to be enclosed within a well stack vented shipping container that must be remotely operated by students, faculty, and personnel from a separate control room shipping container. The bearing under test would be fitted up, have initial tests done, and then closed. The top-level PLC is a Safety Master controller. The system for high-temperature/high-pressure sCO_2 would utilize horizontal split bearings and motor for the parts that are not under test. And if possible, any bearing that can be horizontally split, would be split, so that it fits over the shaft this includes active PM biased magnetic bearings. This won't work for all bearings scheduled to be tested but for active PM biased magnetic bearings we have found ways to split them horizontally so they can fit over the shaft much like stator components within modern compressor/turbine arrangements. The pressure/thermal barrier casing won't be horizontally split but would be of the cartage type where the assembled test bundle is slid inside the moving casing for heated/pressurized testing.

This configuration is found in modern turbomachinery design and has proven to be useful in cost savings, safety, manufacturing, and operation controller. The system for high-temperature/high-pressure sCO_2 would utilize horizontal split bearings and motor for the parts that are not under test. And if possible, any bearing that can be horizontally split, would be split, so that it fits over the shaft this includes active PM biased magnetic bearings. This won't work for all bearings scheduled to be tested but for active PM biased magnetic bearings we have found ways to split them horizontally so they can fit over the shaft much like stator components within modern compressor/turbine arrangements. The pressure/thermal barrier casing won't be horizontally split but would be of the cartridge type where the assembled test bundle is slid inside the moving casing for heated/pressurized testing.

Splitting internal components horizontally makes fabrication, alignment, testing, and repair easier. This concept is somewhat like a split tilt pad bearing already used in turbomachinery. This split configuration may be used for the future application of the tested and approved bearings to be used within application sCO_2 turbomachinery. By extension the split bearings may augment the installation of the application stator/rotor aerodynamic blading assembly and testing.

A heated enclosure would be used to bring the bearing under test within the desired environment. By isolating this bearing from all the rest of the components we can save energy and cost. What this means is that the bearing under test be within an enclosure within the pressure containing casing. This way the pressure containing casing would operate at the same pressure but significantly lower temperature. We find this method used within pressure vessel design where higher temperatures and pressures are found. In pressure vessels this boundary is in many cases refractory. Sometimes this is a metal boundary. This metal boundary sees the high temperature and the pressure, but the pressure is in equilibrium on this interior boundary, so the enclosure only sees thermal induced stress. Likewise, the outer pressure containing boundary sees much less of the thermal load, which facilitates feedthrough bulkhead connectors operating at lower temperatures, and keeps the wall thicknesses thinner for a given ASME boiler code design in most cases.

The horizontal splitable system is shown at the top of the next page and the individual components would be described further in the report. One of the bearings not used in the test is shown with one half removed. The outer thermal containment boundary can be seen enclosing a combination active magnetic bearing. We have made semitransparent one half of the containment enclosure for illustration of the system.

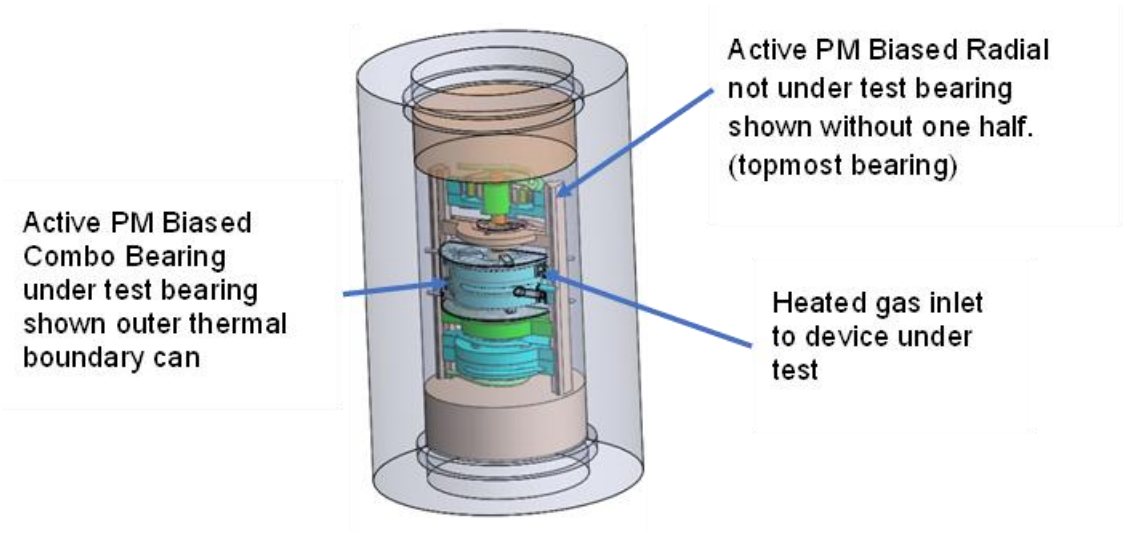

Figure 27: Example Load for the Test System.

Two versions of the horizontal split half bearings were considered. One bearing would have cooling and the hot environment provided by sCO_2. In the alternative version we would use a different cooling gas. Our preferred method was to use sCO_2 as the cooling gas and heating since it so simplifies the system. Sealing is much less of an issue. Canning the dual gas method is also more difficult with a dual gas version.

An autoclave was developed to answer the question on whether we need to use a different cooling gas, or can we use sCO_2. Since sCO_2 when pure is non-conductive there is hope that this would be the best solution. For the radial test system bearings that support the shaft for the device under test they would be cooled to protect the PM bias magnets. However, the rest of the components not part of the bearing under test would not need cooling. For example, the thrust actuator bearing is an EM thrust bearing with no PM bias. Doing this would help keep the focus on the device under test and speed up the process of testing. Likewise, the switched reluctance motor that rotates the shaft up to 30,000 would be a simple construction that the stator splits horizontally and makes testing simpler.

Figure 28 shows the pressure containment casing is of a simple mono block fabrication. All feedthroughs go through both ends only. We have been working with multiple vendors for the autoclave vessel as well as the bearing test vessel. Some of the details took longer to finalize since much redesign was being done on internal components.

Notice the two vertical columns? These are where the horizontally split halves mate to the support structure. There is an adjustment procedure that would allow us to make the bearings concentric to the axis much easier than was achieved. The buildup of the system can be seen in Figure 28 below.

The top and bottom end closures are critical to how the system works. The test device is supported during assembly from the top end plug closure by the main support rails. But to increase the stiffness halves of an outer thin metal cover is bolted to the main support rails. This set of outer metal covers is also useful for covering and holding in place refractory material within the vessel. This refractory helps reduce heat loss, lower vessel wall temperatures, and most especially it reduces the volume of sCO_2 within the system for safety.

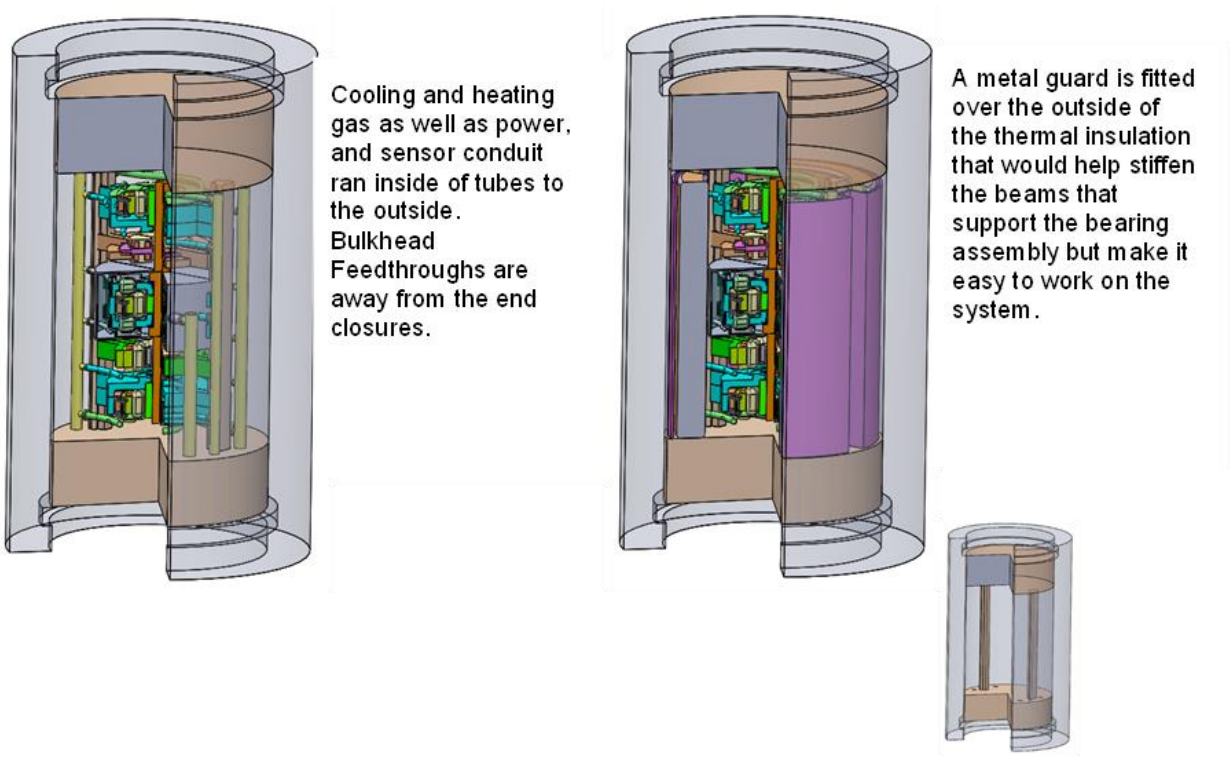

Figure 28: Buildup of a testing package for bearings. This example is for the testing of an active PM biased combination radial and axial bearing

Most of the gas piping as well as the electrical feed throughs are located within the top plug closure. By this method moving the vessel walls would not require extra lengths in the piping or electric cabling.

Shown in Figure 29 are components used during a test on a combo bearing. It would be in the hot containment box. It has features that allow stiffness and damping to be measured by the displacement sensor that are fixed to the non-moving part of the housing and directed to the back outer portion target area.

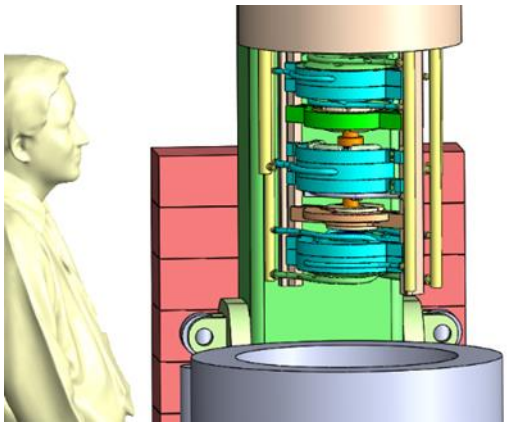

Figure 29: Orientation of Test Rig

SUMMARY

The results of the study demonstrated the feasibility of utilizing permanent magnet biased, fail safe magnetic bearings for sCO_2 turbine shaft support. Reducing the size of the bearing is facilitated by usage of bearing cooling to lower the temperature, and thereby increase the magnetic strength of the permanent magnets. Use of sCO_2 as the coolant was shown to be advantageous over air and N_2. A test rig was designed, and autoclave built for testing a sub-scale sCO_2 turbine demonstrator with magnetic bearing supports, and for testing materials for corrosion in high-temperature and high-pressure sCO_2. Unfortunately, the project work occurred during the COVID shut down era, resulting in incompletion of the test rig. We hope future funding will be forthcoming in order to complete the rig for developing sCO_2 turbine magnetic bearings.

REFERENCES

1. Chapman, P., "Advanced Gas Foil Bearing Design for Supercritical CO2 Power Cycles", 2016 University Turbine Systems Research Workshop November 1-3, 2016 Blacksburg, VA. https://www.netl.doe.gov/File%20Library/Events/2016/utsr/Wednesday/Chapman.pdf
2. Preuss, J., "Application of Hydrostatic Bearings in Supercritical CO2 Turbomachinery", The 5th International Supercritical CO2 Power Cycles Symposium March 29-31, 2016 San Antonio, TX
3. Palazzolo, A., Choi, H., Provenza, A. et.al., "High Temperature, Permanent Magnet Biased, Fault Tolerant, Homopolar Magnetic Bearing Development", *GT2008-50917,* Proceedings of ASME Turbo Expo 2008: Power for Land, Sea and Air, GT 2008, June 9-13, 2008, Berlin, Germany
4. Jinfang Liu[a], Heeju Choi, Alan Palazzolo, Randall Tucker, Andrew Kenny, Kyung-Dae Kang, Varun Ghandi, and Andrew Provenza, "High Temperature Hybrid Radial Magnetic Bearing Systems Capable of Operating up to 538°C (1000°F)", 20th International Workshop on Rare Earth Magnets and Their Applications (REPM08), Greece, EEC Conference Paper REPM08, Sept. 8-10, 2008.
5. Cha, J., Cho, S., and Lee J., "Operation Test of the Supercritical CO2 Compressor Supported with Active Magnetic Bearing", Transactions of the Korean Nuclear Society Autumn Meeting Gyeongju, Korea, October 27-28, 2016
6. Provenza, A., Montague, G., Jansen, M., Palazzolo, A., and Jansen, R., "High Temperature Characterization of a Radial Magnetic Bearing for Turbomachinery," J. of Engineering for Gas Turbines and Power , v 127, n 2, April, 2005, p 437-444
7. Zhong*, W., and Palazzolo, A., "Magnetic Bearing Rotordynamic System Optimization Using Multi-Objective Genetic Algorithms", ASME J. of Dynamic Systems, Measurement and Control, 137(2), Feb. 2015
8. Wan Zhong* , Alan Palazzolo and Xiao Kang, "Multi-Objective Optimization Design of Nonlinear Magnetic Bearing Rotordynamic System", ASME J. Vib. Acoust 139(1), Feb. 2017
9. Li*, Ming Hsiu, Palazzolo,A., Kenny*, A., Provenza, A., Beach,R., Kascak,A., "Fault Tolerant Homopolar Magnetic Bearings", IEEE Trans. On Magnetics, Vol. 40, No. 5, Sept. 2004, pp. 3308–3318.
10. "Fault Tolerant Homopolar Magnetic Bearings", *U.S. Patent 7,429,811,*Date of Patent 30 September 2008, Co Inventors: Palazzolo, Hsiu Li, Kenny, Beach, Kascak , Provenza, Tucker. http://patft.uspto.gov/netahtml/PTO/srchnum.htm

11. Kim*, C., Palazzolo, A., Kascak, A. and Brown, G., “Eddy Current Effects On the Design of Rotor Magnetic Bearing Systems”, ASME Special 50th Anniversary Design Issue, June 1995, Vol. 117, pp. 162-170.

12. Chinta*, M., and Palazzolo, A., “Stability and Bifurcation of Rotor Motion in a Magnetic Bearing,” J. of Sound and Vibration, 1998, 214(5), 793-803.

13. DeWeese*, R., Palazzolo, A. and Chinta*, M. and Kascak, A., “Magnetic Thrust Bearing Concepts: Tests and Analysis”, J. Intelligent Materials, Systems and Structures, Vol. 9, No. 2, Feb. 1998, pp. 81-86.

14. Na*, U.J. and Palazzolo, A.B., “Optimized Realization of Redundant Heteropolar Magnetic Bearings,” ASME J. of Vibrations, July 2000, Vol. 122, pp. 209-221.

15. Lei*, S., Palazzolo, A. and Kascak, A., “Nonlinear Fuzzy Logic Control for Forced Large Motions of Spinning Shafts.” J. of Sound and Vibrations, Vol. 235(3), 17 August 2000, pp. 435-449.

16. Na*, U.J. and Palazzolo, A.B., “Fault Tolerance of a Magnetic Bearing Including Material Path Reluctances and Fringe Factors”, IEEE Journal for Magnetics, Nov. 2000, Vol. 36, No. 6.

17. Na*, U.J., Palazzolo, A.B., “The Fault Tolerant Control of Magnetic Bearings with Reduced Controller Outputs”, ASME J. Dynamic Syst., Meas. and Controls, June 2001, Vol. 123, pp. 219-224.

18. Pichot, M., Kajs, J., Murphy B., Ouroua, A., Rech, R., Hayes, R., Bens, J., Buckner, G. and Palazzolo, A., “Active Magnetic Bearings for Energy Storage Systems for Combat Vehicles,” IEEE Transactions on Magnetics, Vol. 37, No. 1, January 2001, pp. 318-323.

19. Kenny*, A. and Palazzolo, A., “Comparison of the Dynamic Response of Radial and Tangential Magnetic Flux Thrust Bearings”, IEEE/ASME Trans. on Mechatronics, Vol. 7, No. 1, March 2002.

20. Na*, U.J., Provenza, A., Palazzolo, A.B., Montague, G. and Kascak, A., “Test and Theory Correlation Study for a Flexible Rotor on Fault-Tolerant Magnetic Bearings,” ASME Journal of Vibration and Acoustic, 124(3):359-366, Jul. 2002.

21. Kenny*, A. and Palazzolo, A., “Single Plane Radial, Magnetic Bearings Biased with Poles Containing Permanent Magnets,” ASME J. of Mechanical Design, March 2003, Vol. 125, pp. 178-185.

22. Minihan*, T., Lei*, S., Sun*, G. and Palazzolo, A., “Large Motion Tracking Control for Thrust Magnetic Bearings With Fuzzy Logic, Sliding Mode, and Direct Linearization,” Journal of Sound and Vibration, 263 (2003), 549-567.

23. Sun*, G., Palazzolo, A., Provenza, A. and Montague, G., “Detailed Ball Bearing Model for Magnetic Suspension Auxiliary Service”, J. of Sound and Vibration, Vol. 269, Issues 3-5, 22 January 2004, pp. 933-963.

24. Kenny*, A., Palazzolo, A., Montague, G. and Kascak, A., “Theory and Test Correlation for Laminate Stacking Factor Effect on Homopolar Magnetic Bearing Stiffness”, ASME J. of Engineering for Gas Turbines and Power, Vol. 126, January 2004, pp. 142-146.

25. Li*, Ming Hsiu, Palazzolo,A., Kenny*, A., Provenza, A., Beach,R., Kascak,A., “Fault Tolerant Homopolar Magnetic Bearings”, IEEE Trans. On Magnetics, Vol. 40, No. 5, Sept. 2004, pp. 3308–3318.

26. Guangyoung Sun*, Alan B. Palazzolo, ‘‘Rotor drop and following thermal growth simulations

using detailed auxiliary bearing and damper models'', J. Sound and Vibration 289 (2006) 334–359, Note: Corrigendum for authors was published in Journal of Sound and Vibration 306 (2007) 975.

27. Lei*, Shuliang and Palazzolo, A., "Control of Flexible Rotor Systems with Active Magnetic Bearings", J. Sound and Vibrations, 8 July 2008, Vol. 314, pp. 19-38
28. Kang*, K., and Palazzolo, A.B., Homopolar Magnetic Bearing Saturation Effects on Rotating Machinery Vibration, IEEE Trans. on Magnetics, June 2012, Vol. 48, No. 6, pp. 1984-1994.
29. Lee*, Jung Gu, and Palazzolo, A., " Catcher Bearing Life Prediction Using a Rainflow Counting Approach", ASME J. of Tribology, July 2012 -- Volume 134, Issue 3, 031101 (15 pages).
30. Kang, Xiao and Palazzolo, A., "Dynamic and Thermal Analysis of Rotor Drop on Sleeve Type Catcher Bearings in Magnetic Bearing Systems", ASME Journal of Engineering for Gas Turbines and Power, Feb. 2018, Vo. 140, Issue 2
31. Kang, Xiao, Palazzolo, A., "Auxiliary Bearing Squeeze Film Dampers for Magnetic Bearing Supported Rotors", Tribology International, Vol. 146, June 2020
32. Kang*, X., and Palazzolo, A.,"Simulation, Test and Mitigation of 1/2x Forward Whirl Following Rotor Drop onto Auxiliary Bearings, GT2019-91645, ASME J. of Engineering and Gas Turbines for Power, April 2020

ACKNOWLEDGEMENTS

This work is based upon work supported by the U.S. Department of Energy, Office of Nuclear Energy, under Award Number SC0018813. This financial assistance from Department of Energy is gratefully acknowledged.